Electronic Supplementary Information

Solvent-effect-driven assembly of W/Cu/S cluster-based coordination polymers from the cluster precursor $[Et_4N][Tp^*WS_3(CuBr)_3]$ and CuCN: isolation, structures and enhanced NLO responses

Quan Liu,[ad] Zhi-Gang Ren,[a] Li Deng,[c] Wen-Hua Zhang,*[a] Li-Kuan Zhou,[a] Xin Zhao,[a] Zhen-Rong Sun,[c] and Jian-Ping Lang*[ab]

[a] *College of Chemistry, Chemical Engineering and Materials Science, Soochow University, Suzhou 215123, P. R. China*

[b] *Shanghai Institute of Organic Chemistry, Chinese Academy of Science, Shanghai 200032, P. R. China*

[c] *Department of Physics, East China Normal University, Shanghai 200062, P. R. China*

[d] *College of Chemistry and Chemical Engineering, Nantong University, Nantong 226019, P. R. China*

Table of Contents

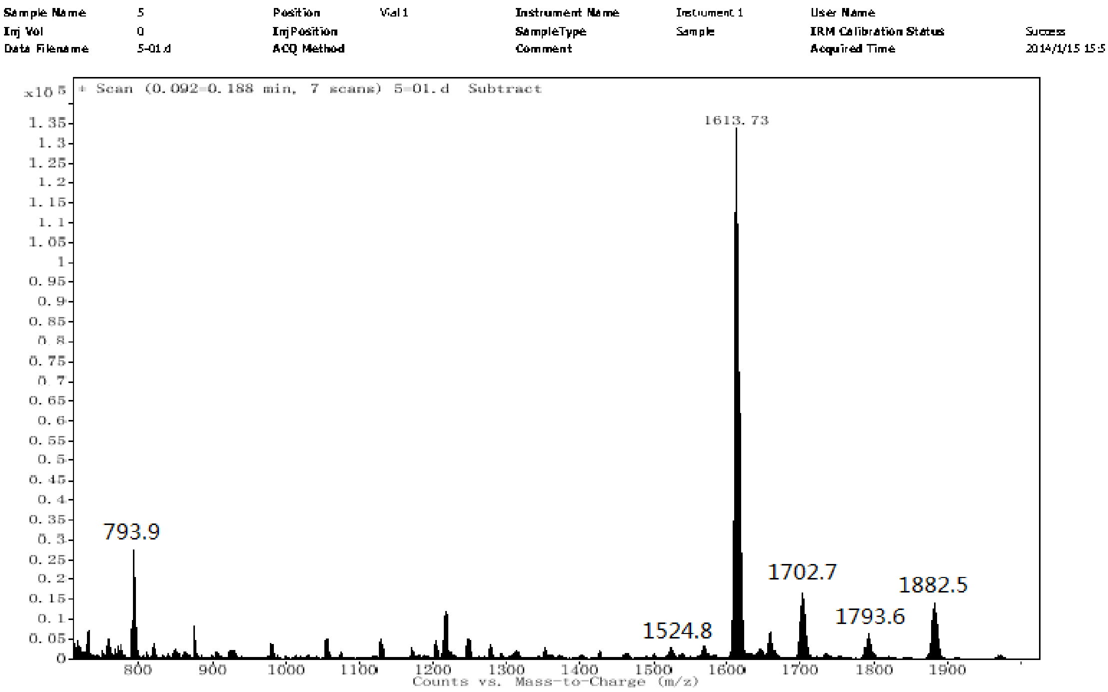
Sample Name 5
Position Vial 1
Instrument Name Instrument 1
User Name
Inj Vol 0
InjPosition
SampleType Sample
IRM Calibration Status Success
Data Filename 5-01.d
ACQ Method
Comment
Acquired Time 2014/1/15 15:5
+ Scan (0.092-0.188 min, 7 scans) 5-01.d Subtract
x10 5
1613.73
793.9
1702.7
1882.5
1793.6
1524.8
Counts vs. Mass-to-Charge (m/z)

(a)

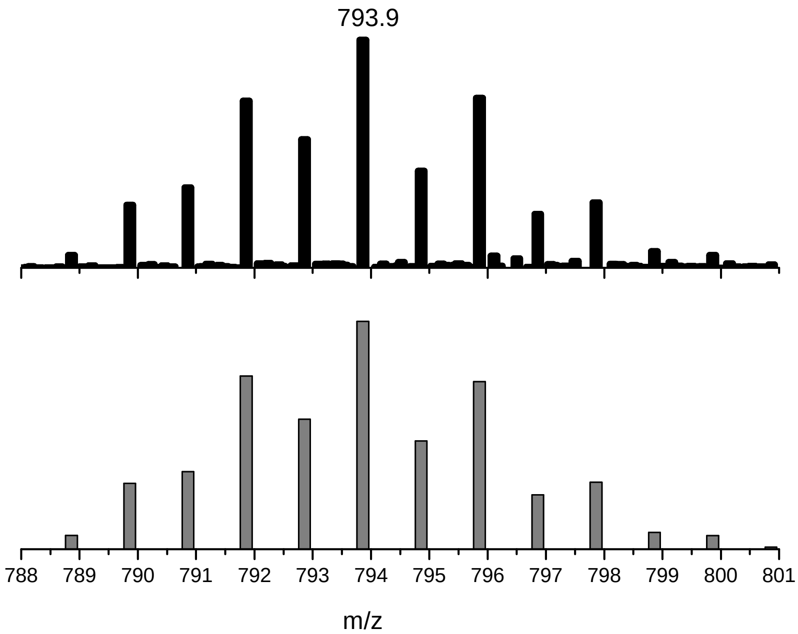
793.9
788
789
790
791
792
793
794
795
796
797
798
799
800
801
m/z

(b)

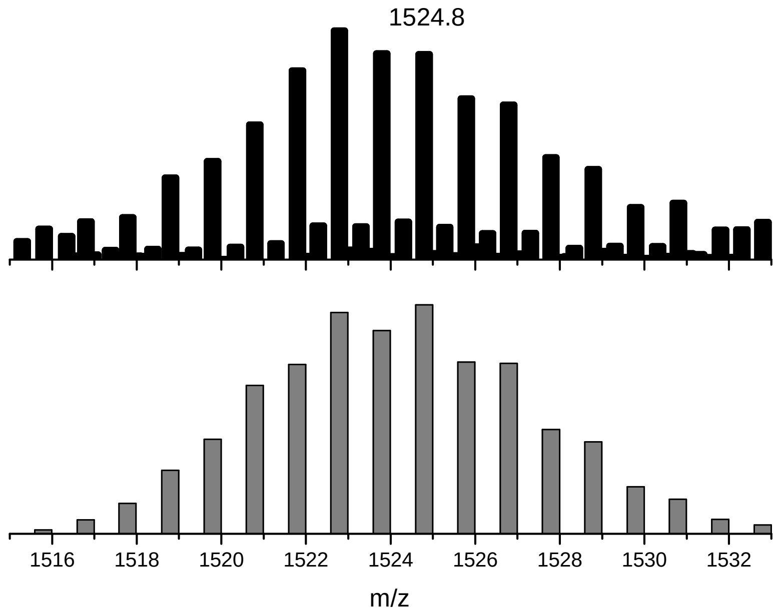
1524.8
1516
1518
1520
1522
1524
1526
1528
1530
1532
m/z

(c)

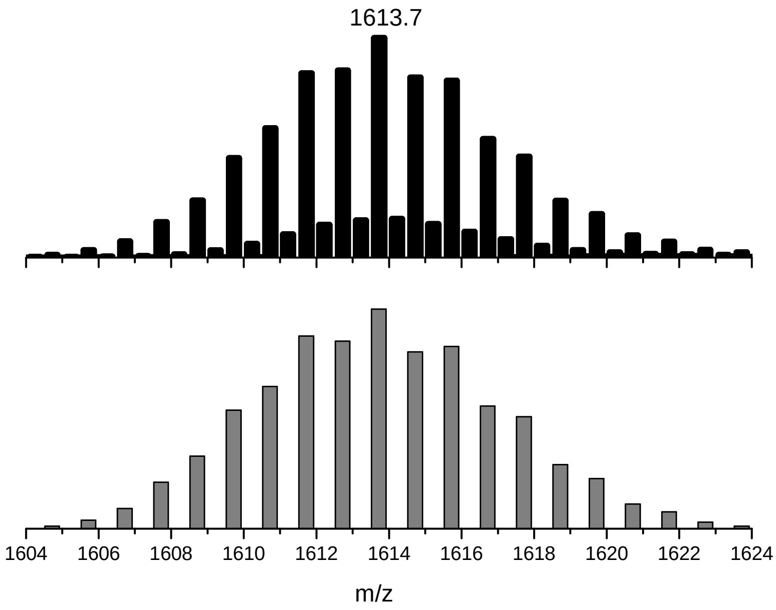
1613.7
1604
1606
1608
1610
1612
1614
1616
1618
1620
1622
1624
m/z

(d)

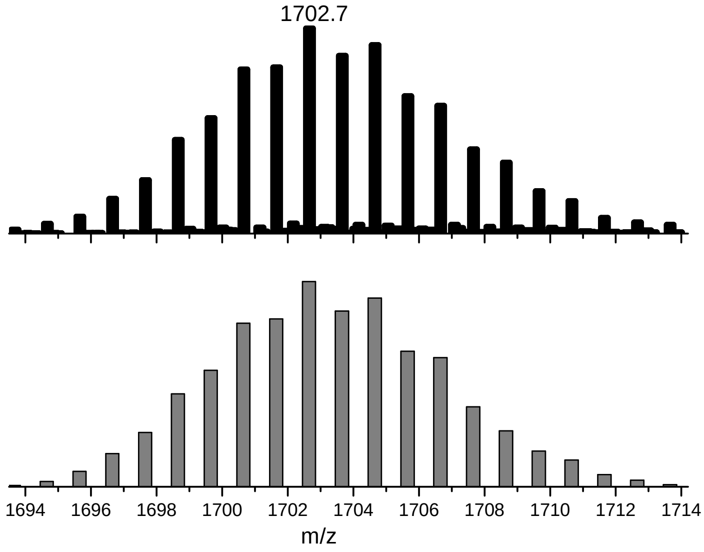
1702.7
1694
1696
1698
1700
1702
1704
1706
1708
1710
1712
1714
m/z

(e)

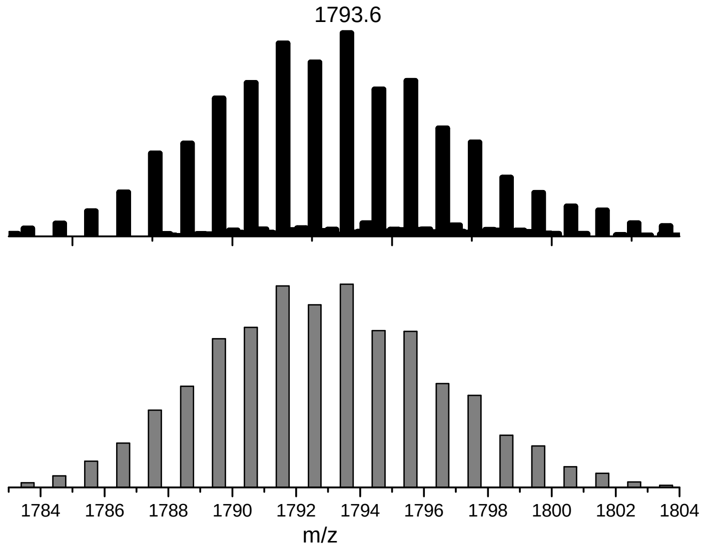
1793.6
1784
1786
1788
1790
1792
1794
1796
1798
1800
1802
1804
m/z

(f)

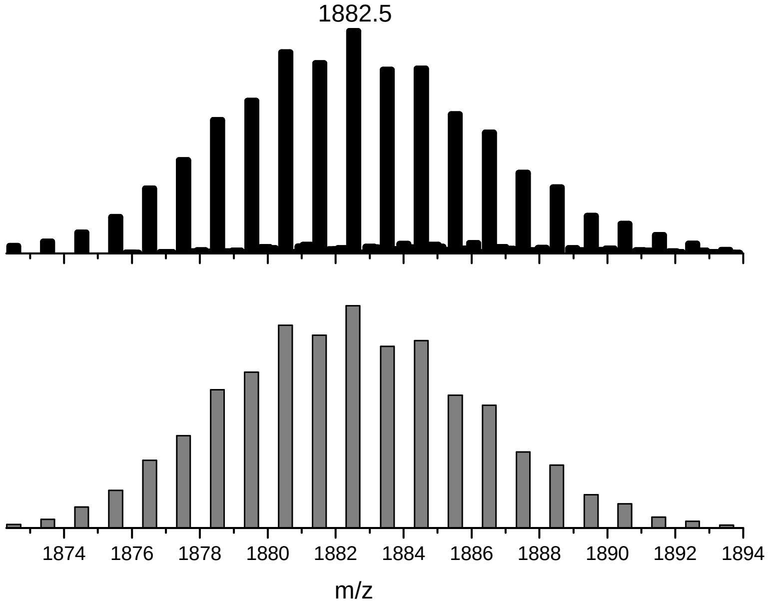

(g)

Fig. S1 (a) The positive-ion ESI mass spectrum of [Tp*WS_3Cu_3(μ_3-DMF)$(CN)_3$Cu(Py)] (**2**). (b) The observed patterns (up) and the calculated isotope patterns (bottom) of the $[Tp^*WS_3Cu_3(CN)]^+$ cation (at m/z = 793.9). (c) The observed patterns (up) and the calculated isotope patterns (bottom) of the $[(Tp^*WS_3Cu_2)(Tp^*WS_3Cu_3)(CN)_2]^+$ cation (at m/z = 1524.8). (d) The observed patterns (up) and the calculated isotope patterns (bottom) of the $[(Tp^*WS_3Cu_3)_2(CN)_3]^+$ cation (at m/z = 1613.7). (e) The observed patterns (up) and the calculated isotope patterns (bottom) of the $[(Tp^*WS_3Cu_3)_2Cu(CN)_4]^+$ cation (at m/z = 1702.7). (f) The observed patterns (up) and the calculated isotope patterns (bottom) of the $[(Tp^*WS_3Cu_3)_2Cu_2(CN)_5]^+$ cation (at m/z = 1793.6). (g) The observed patterns (up) and the calculated isotope patterns (bottom) of the $[(Tp^*WS_3Cu_3)_2Cu_3(CN)_6]^+$ cation (at m/z = 1882.5).

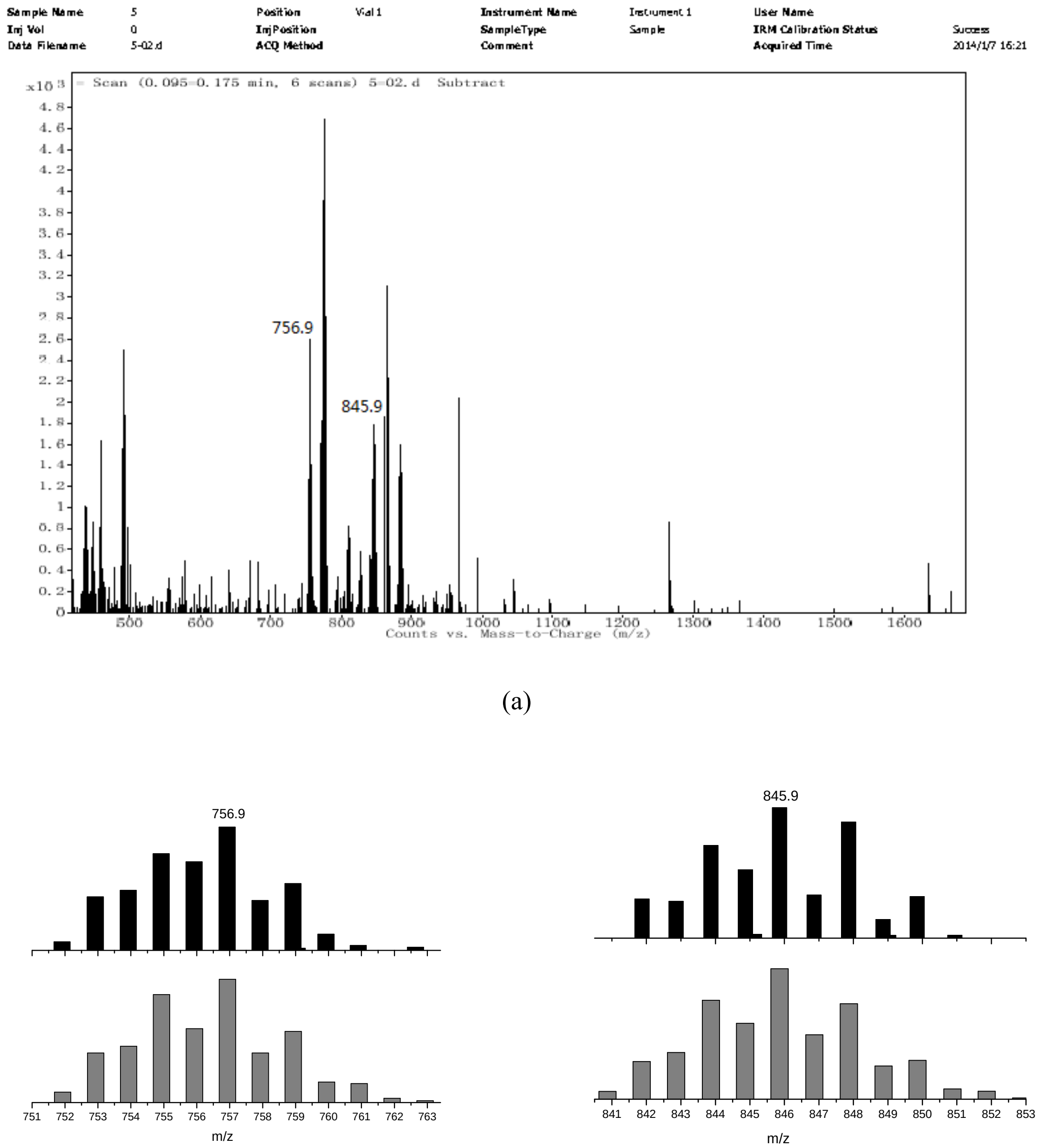

(a)

(b)

(c)

Fig. S2 (a) The negative-ion ESI mass spectrum of [Tp*WS_3Cu_3(μ_3-DMF)$(CN)_3$Cu(Py)] (**2**). (b) The observed patterns (up) and the calculated isotope patterns (bottom) of the [Tp*$WS_3Cu_2(CN)_2$]$^-$ anion (at m/z = 756.9). (c) The observed patterns (up) and the calculated isotope patterns (bottom) of the [Tp*$WS_3Cu_3(CN)_3$]$^-$ anion (at m/z = 845.9).

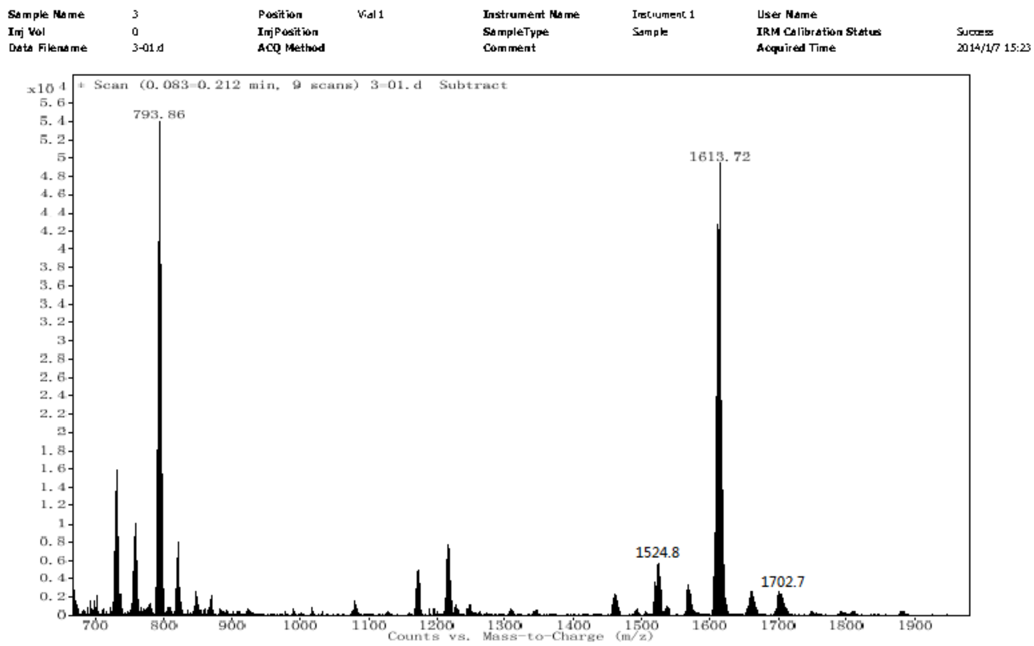
Sample Name 3
Position Vial 1
Instrument Name Instrument 1
User Name
Inj Vol 0
InjPosition
SampleType Sample
IRM Calibration Status Success
Data Filename 3-01.d
ACQ Method
Comment
Acquired Time 2014/1/7 15:23
+ Scan (0.083-0.212 min, 9 scans) 3-01.d Subtract
793.86
1613.72
1524.8
1702.7
Counts vs. Mass-to-Charge (m/z)

(a)

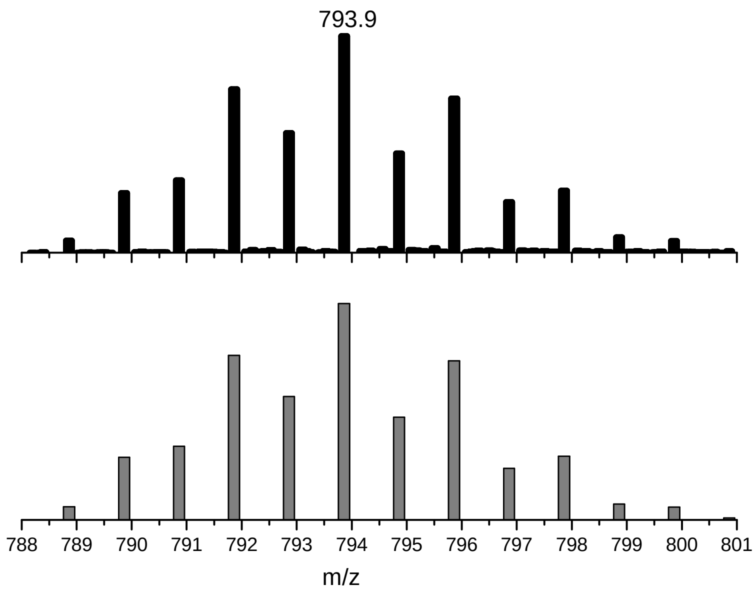
793.9
788
789
790
791
792
793
794
795
796
797
798
799
800
801
m/z

(b)

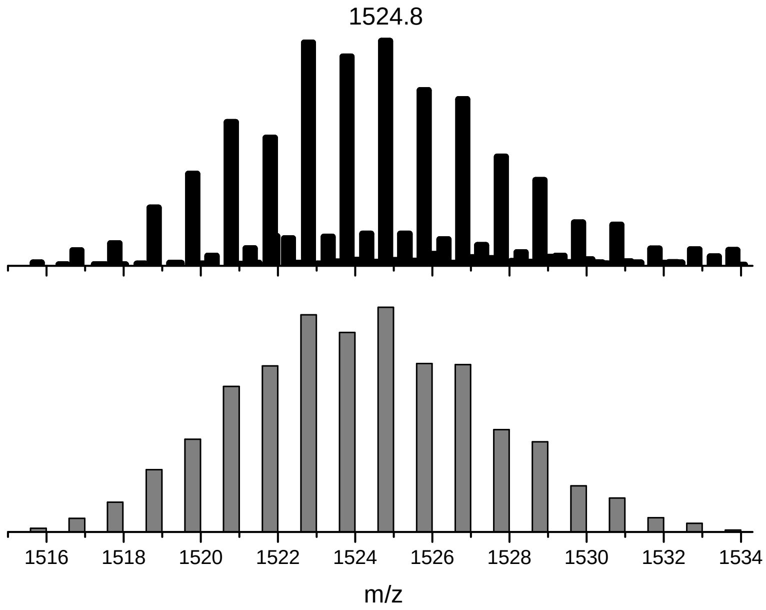
1524.8
1516
1518
1520
1522
1524
1526
1528
1530
1532
1534
m/z

(c)

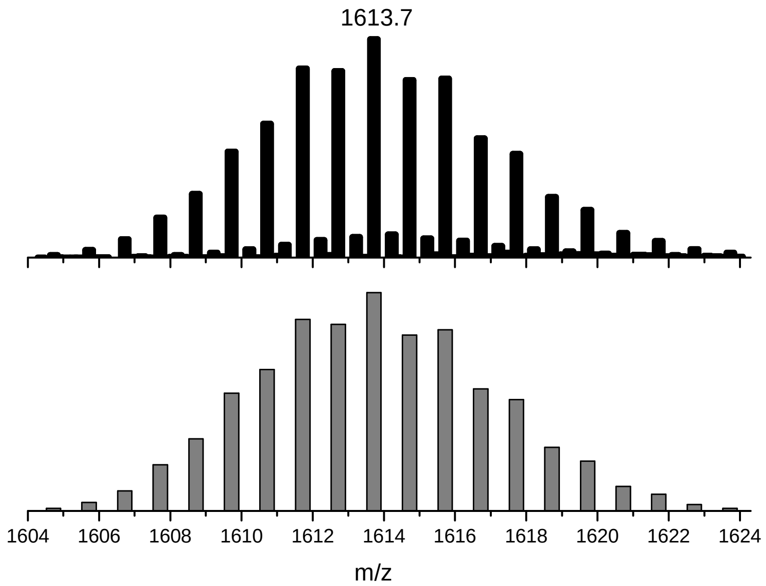
1613.7
1604
1606
1608
1610
1612
1614
1616
1618
1620
1622
1624
m/z

(d)

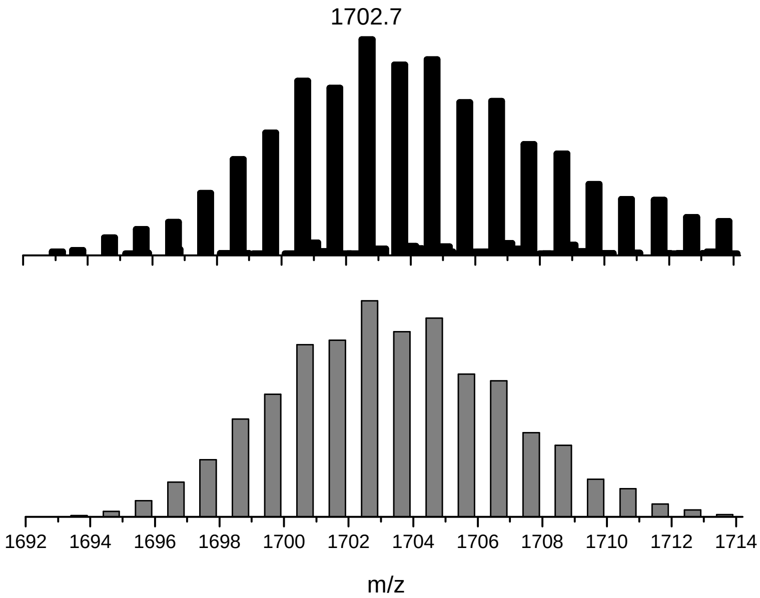

(e)

Fig. S3 (a) The positive-ion ESI mass spectrum of [Tp*$WS_3Cu_3(\mu_3$-DMF)$(CN)_3$Cu] (**3**). (b) The observed patterns (up) and the calculated isotope patterns (bottom) of the [Tp*WS_3Cu_3(CN)$]^+$ cation (at m/z = 793.9). (c) The observed patterns (up) and the calculated isotope patterns (bottom) of the [(Tp*WS_3Cu_2)(Tp*WS_3Cu_3)$(CN)_2]^+$ cation (at m/z = 1524.8). (d) The observed patterns (up) and the calculated isotope patterns (bottom) of the [(Tp*$WS_3Cu_3)_2(CN)_3]^+$ cation (at m/z = 1613.7). (e) The observed patterns (up) and the calculated isotope patterns (bottom) of the [(Tp*$WS_3Cu_3)_2$Cu$(CN)_4]^+$ cation (at m/z = 1702.7).

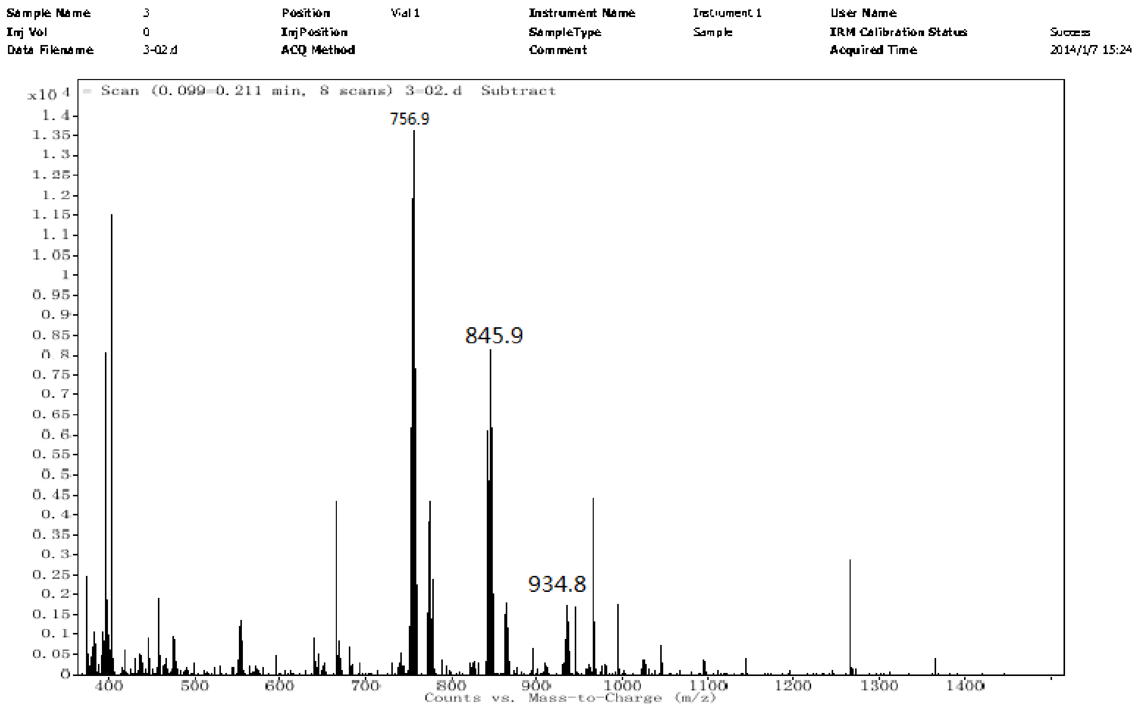
Sample Name 3
Position Vial 1
Instrument Name Instrument 1
User Name
Inj Vol 0
InjPosition
SampleType Sample
IRM Calibration Status Success
Data Filename 3-02.d
ACQ Method
Comment
Acquired Time 2014/1/7 15:24
x10 4
+ Scan (0.099-0.211 min, 8 scans) 3-02.d Subtract
756.9
845.9
934.8
Counts vs. Mass-to-Charge (m/z)

(a)

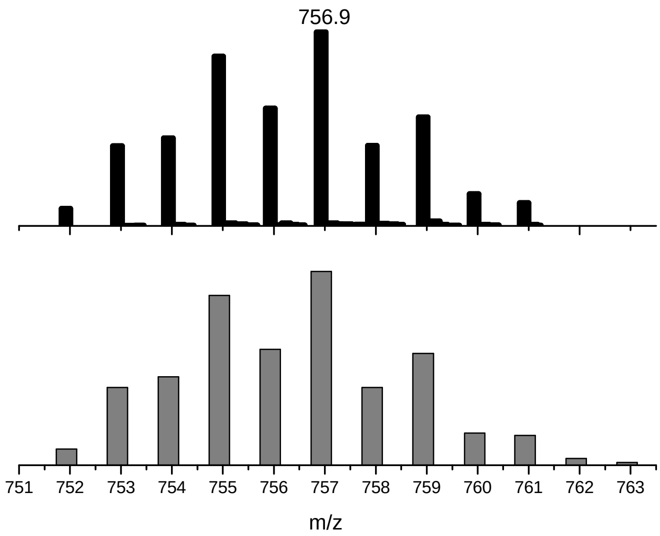
756.9
751
752
753
754
755
756
757
758
759
760
761
762
763
m/z

(b)

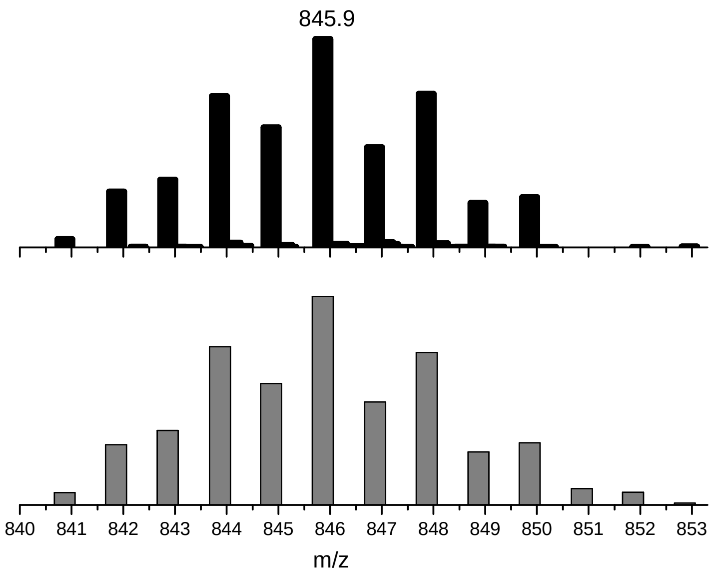

(c)

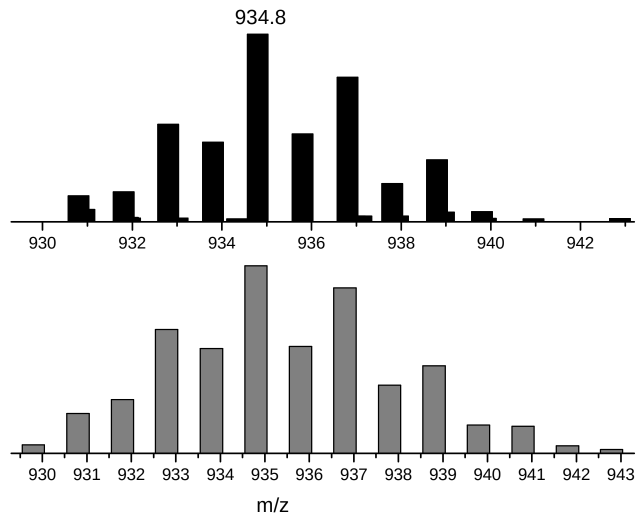

(d)

Fig. S4 (a) The negative-ion ESI mass spectrum of [Tp*WS_3Cu_3(μ_3-DMF)$(CN)_3$Cu] (**3**). (b) The observed patterns (up) and the calculated isotope patterns (bottom) of the [Tp*$WS_3Cu_2(CN)_2]^-$ anion (at m/z = 756.9). (c) The observed patterns (up) and the calculated isotope patterns (bottom) of the [Tp*$WS_3Cu_3(CN)_3]^-$ anion (at m/z = 845.9). (d) The observed patterns (up) and the calculated isotope patterns (bottom) of the [(Tp*WS_3Cu_3)Cu$(CN)_4]^-$ anion (at m/z = 934.8).

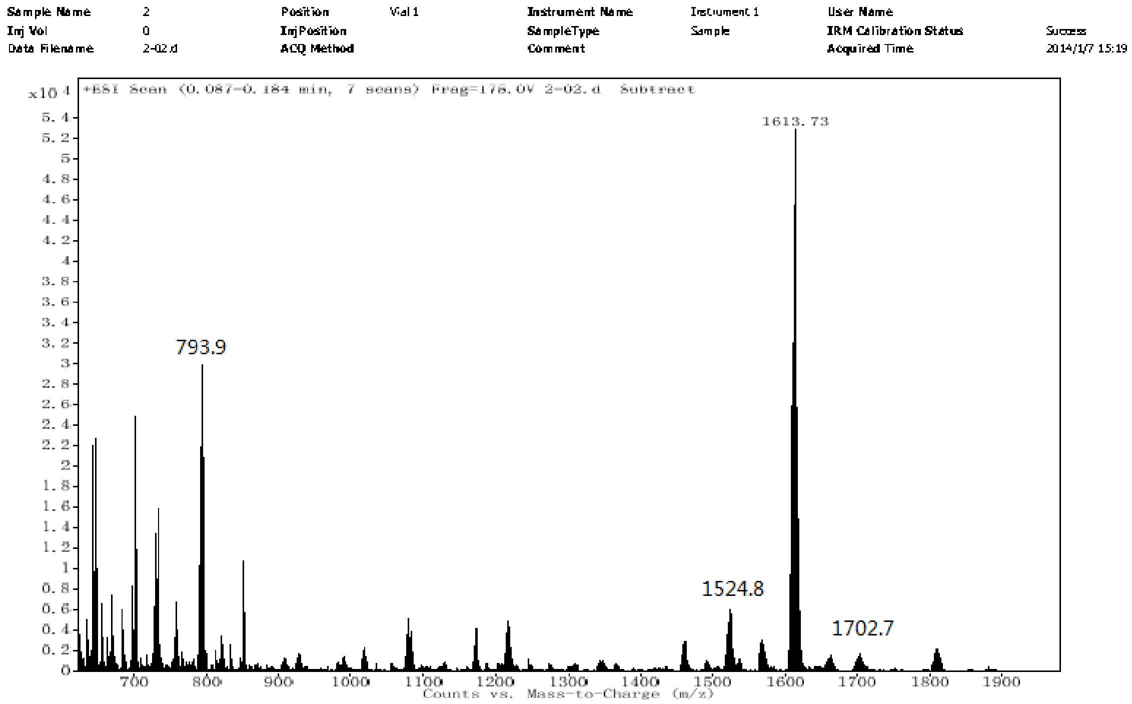
Sample Name 2
Position Vial 1
Instrument Name Instrument 1
User Name
Inj Vol 0
InjPosition
SampleType Sample
IRM Calibration Status Success
Data Filename 2-02.d
ACQ Method
Comment
Acquired Time 2014/1/7 15:19
+ESI Scan (0.087-0.184 min, 7 scans) Frag=175.0V 2-02.d Subtract
1613.73
793.9
1524.8
1702.7
Counts vs. Mass-to-Charge (m/z)

(a)

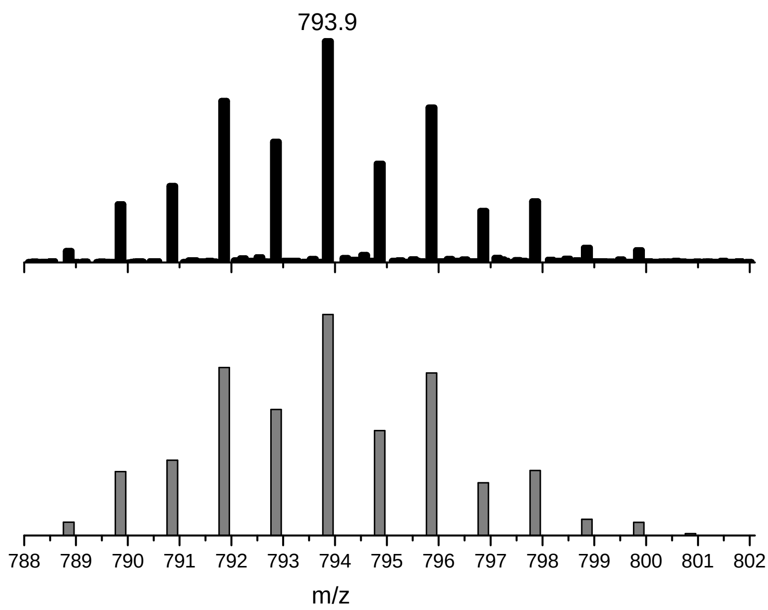
793.9
m/z

(b)

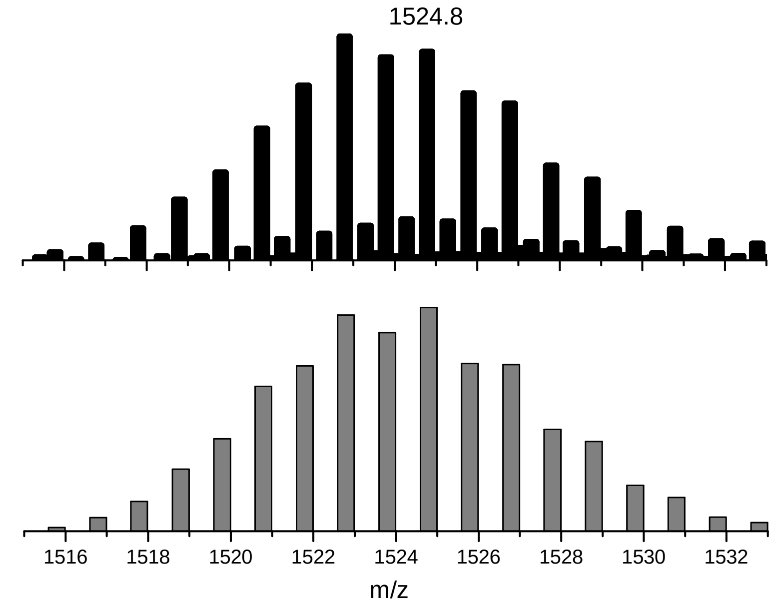
1524.8
1516
1518
1520
1522
1524
1526
1528
1530
1532
m/z

(c)

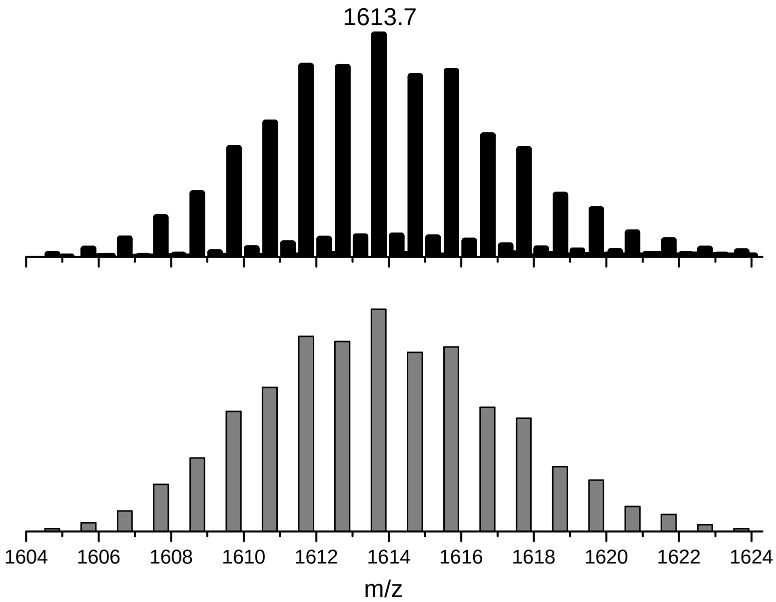
1613.7
1604
1606
1608
1610
1612
1614
1616
1618
1620
1622
1624
m/z

(d)

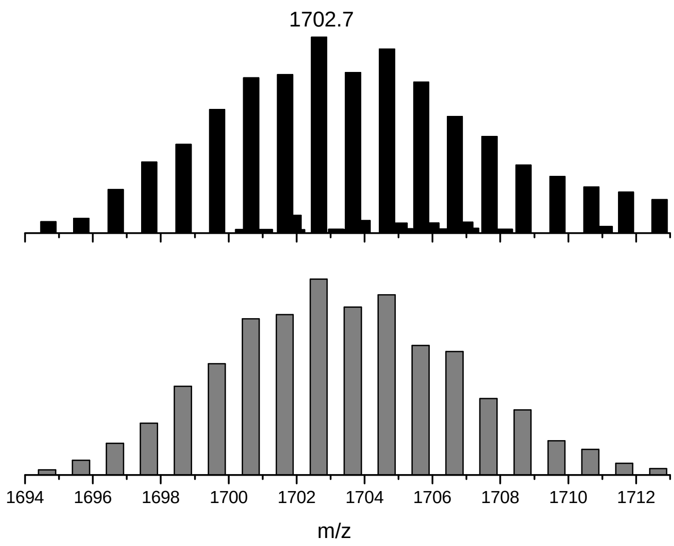

(e)

Fig. S5 (a) The positive-ion ESI mass spectrum of [Tp*WS_3Cu_3(μ_3-DMF)$(CN)_3$Cu]·4aniline (**4**·4aniline). (b) The observed patterns (up) and the calculated isotope patterns (bottom) of the [Tp*WS_3Cu_3(CN)]$^+$ cation (at m/z = 793.9). (c) The observed patterns (up) and the calculated isotope patterns (bottom) of the [(Tp*WS_3Cu_2)(Tp*WS_3Cu_3)$(CN)_2$]$^+$ cation (at m/z = 1524.8). (d) The observed patterns (up) and the calculated isotope patterns (bottom) of the [(Tp*WS_3Cu_3)$_2$$(CN)_3$]$^+$ cation (at m/z = 1613.7). (e) The observed patterns (up) and the calculated isotope patterns (bottom) of the [(Tp*WS_3Cu_3)$_2$Cu$(CN)_4$]$^+$ cation (at m/z = 1702.7).

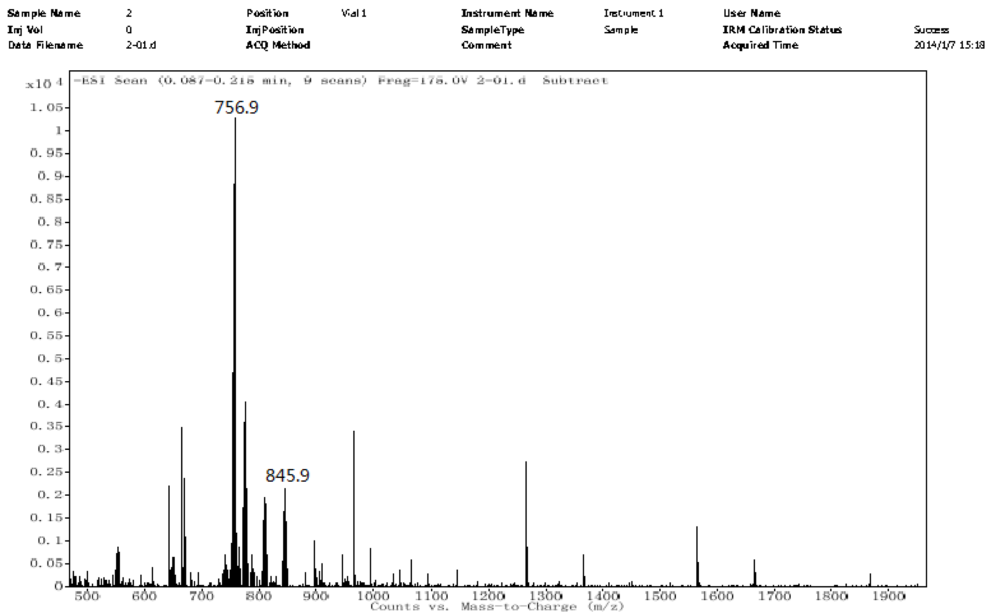

(a)

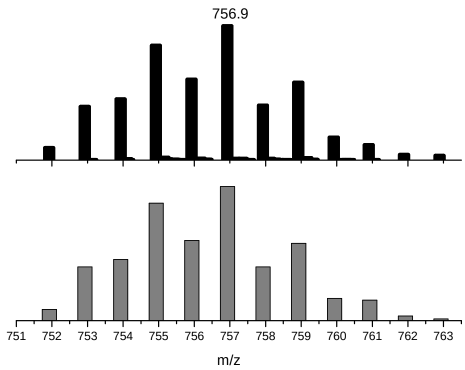

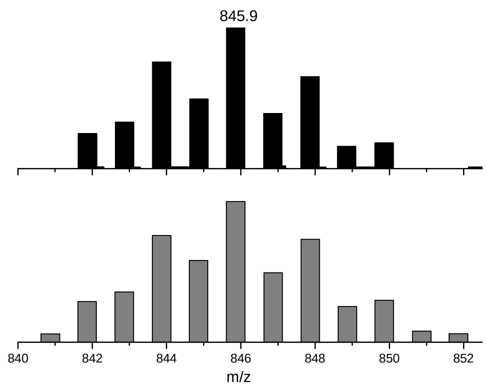

(b) (c)

Fig. S6 (a) The negative-ion ESI mass spectrum of [Tp*WS_3Cu_3(μ_3-DMF)$(CN)_3$Cu]·4aniline (**4**·4aniline). (b) The observed patterns (up) and the calculated isotope patterns (bottom) of the [Tp*$WS_3Cu_2(CN)_2$]$^-$ anion (at m/z = 756.9). (c) The observed patterns (up) and the calculated isotope patterns (bottom) of the [Tp*$WS_3Cu_3(CN)_3$]$^-$ anion (at m/z = 845.9).

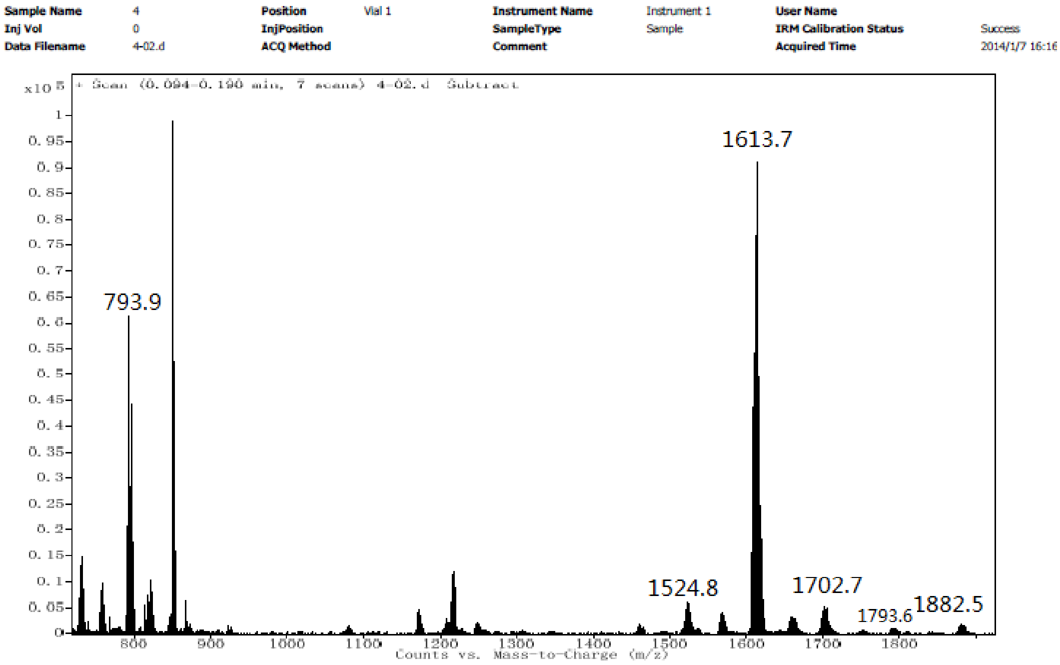

Sample Name 4
Position Vial 1
Instrument Name Instrument 1
User Name
Inj Vol 0
InjPosition
SampleType Sample
IRM Calibration Status Success
Data Filename 4-02.d
ACQ Method
Comment
Acquired Time 2014/1/7 16:16
+ Scan (0.094-0.190 min, 7 scans) 4-02.d Subtract
793.9
1613.7
1524.8
1702.7
1793.6
1882.5
Counts vs. Mass-to-Charge (m/z)

(a)

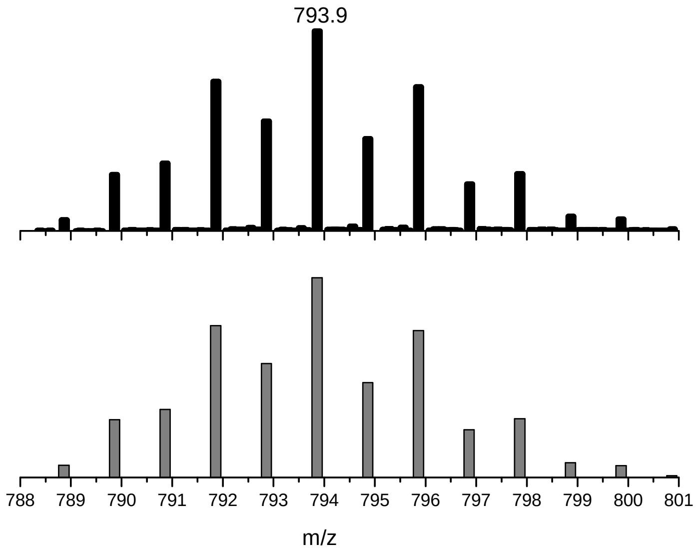

793.9
m/z

(b)

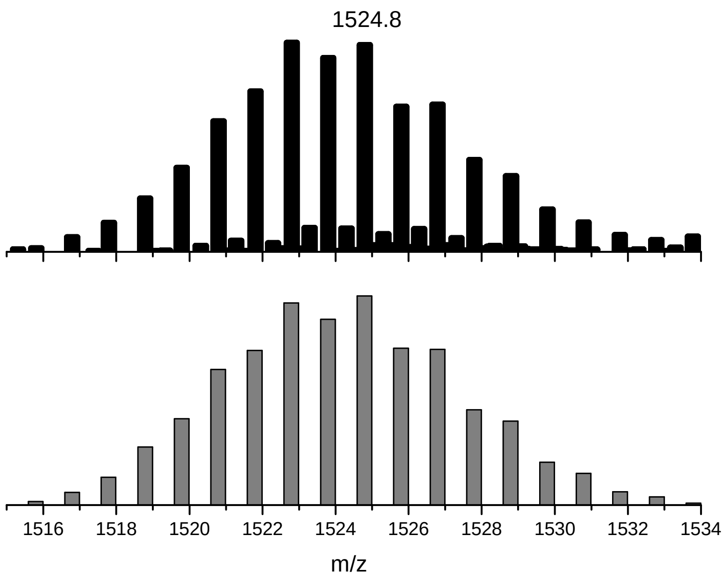
1524.8
1516
1518
1520
1522
1524
1526
1528
1530
1532
1534
m/z

(c)

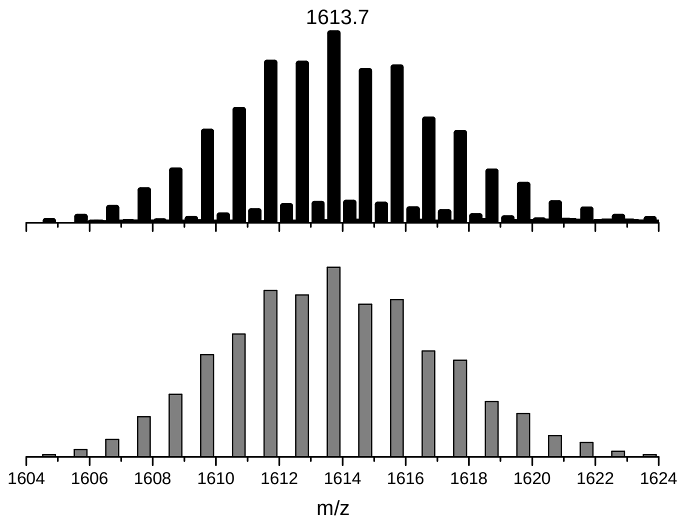
1613.7
1604
1606
1608
1610
1612
1614
1616
1618
1620
1622
1624
m/z

(d)

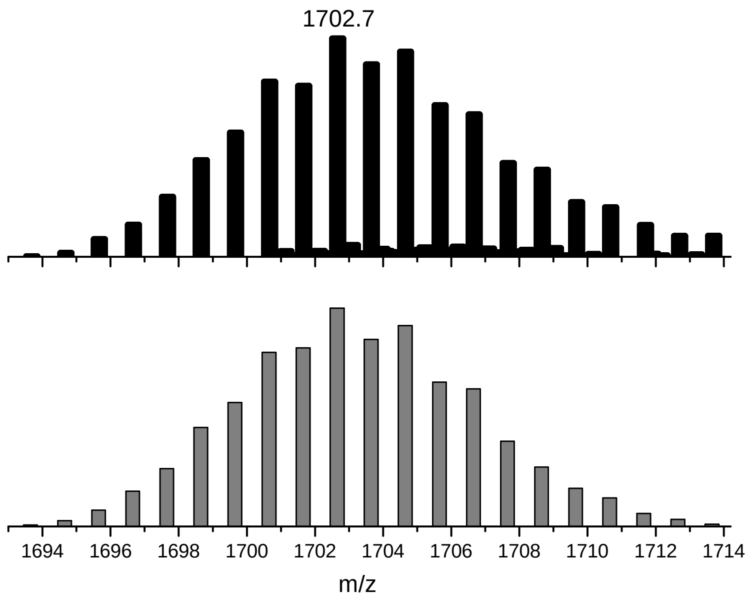
1702.7
1694
1696
1698
1700
1702
1704
1706
1708
1710
1712
1714
m/z

(e)

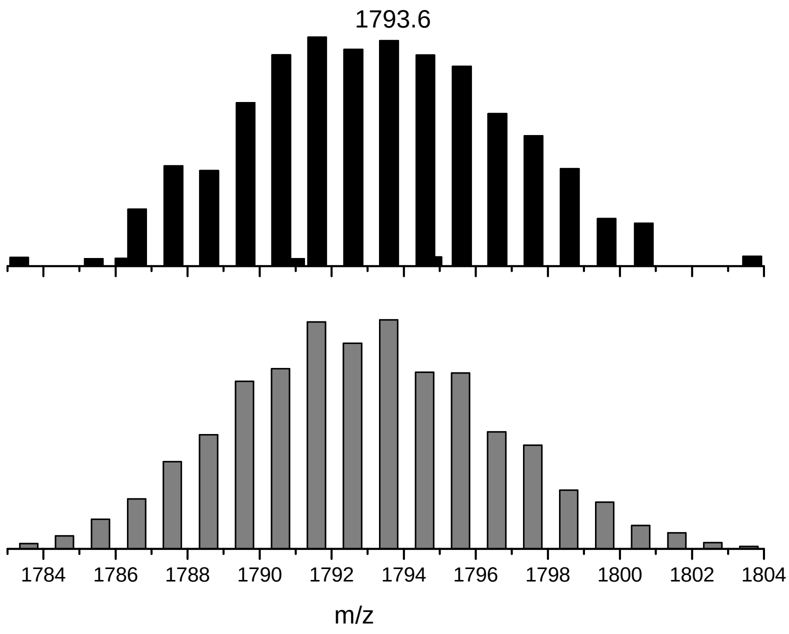
1793.6
1784
1786
1788
1790
1792
1794
1796
1798
1800
1802
1804
m/z

(f)

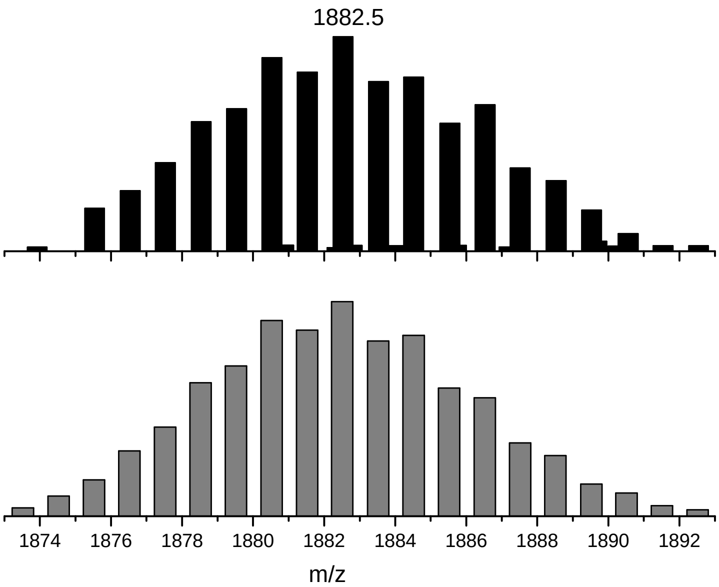

(g)

Fig. S7 (a) The positive-ion ESI mass spectrum of [Tp*WS_3Cu_3(μ_3-DMF)$(CN)_3$Cu]·2$(DMF)_{0.5}$. (b) The observed patterns (up) and the calculated isotope patterns (bottom) of the $[Tp*WS_3Cu_3(CN)]^+$ cation (at m/z = 793.9). (c) The observed patterns (up) and the calculated isotope patterns (bottom) of the $[(Tp*WS_3Cu_2)(Tp*WS_3Cu_3)(CN)_2]^+$ cation (at m/z = 1524.8). (d) The observed patterns (up) and the calculated isotope patterns (bottom) of the $[(Tp*WS_3Cu_3)_2(CN)_3]^+$ cation (at m/z = 1613.7). (e) The observed patterns (up) and the calculated isotope patterns (bottom) of the $[(Tp*WS_3Cu_3)_2Cu(CN)_4]^+$ cation (at m/z = 1702.7). (f) The observed patterns (up) and the calculated isotope patterns (bottom) of the $[(Tp*WS_3Cu_3)_2Cu_2(CN)_5]^+$ cation (at m/z = 1793.6). (g) The observed patterns (up) and the calculated isotope patterns (bottom) of the $[(Tp*WS_3Cu_3)_2Cu_3(CN)_6]^+$ cation (at m/z = 1882.5).

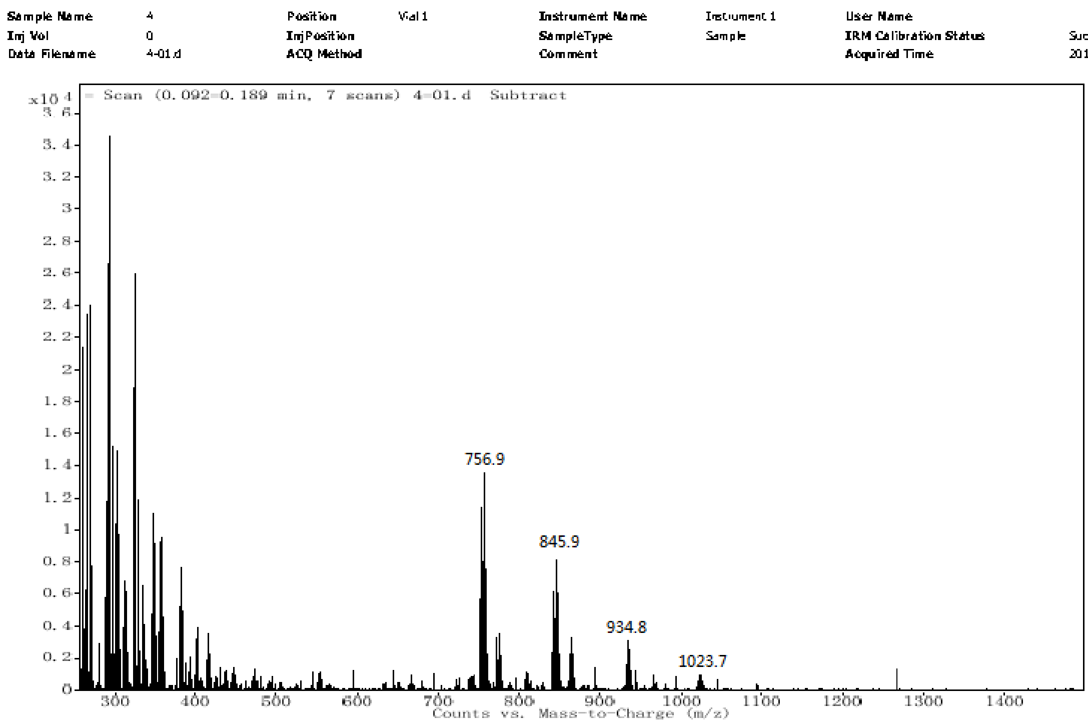
Sample Name 4
Position Vial 1
Instrument Name Instrument 1
User Name
Inj Vol 0
InjPosition
SampleType Sample
IRM Calibration Status Success
Data Filename 4-01.d
ACQ Method
Comment
Acquired Time 2014/1/15 15:5
+ Scan (0.092-0.189 min, 7 scans) 4-01.d Subtract
x10 4
756.9
845.9
934.8
1023.7
Counts vs. Mass-to-Charge (m/z)

(a)

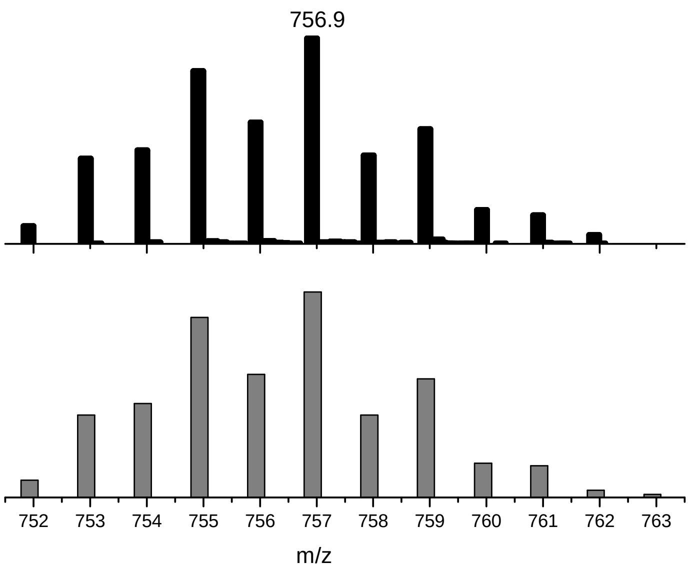
756.9
752
753
754
755
756
757
758
759
760
761
762
763
m/z

(b)

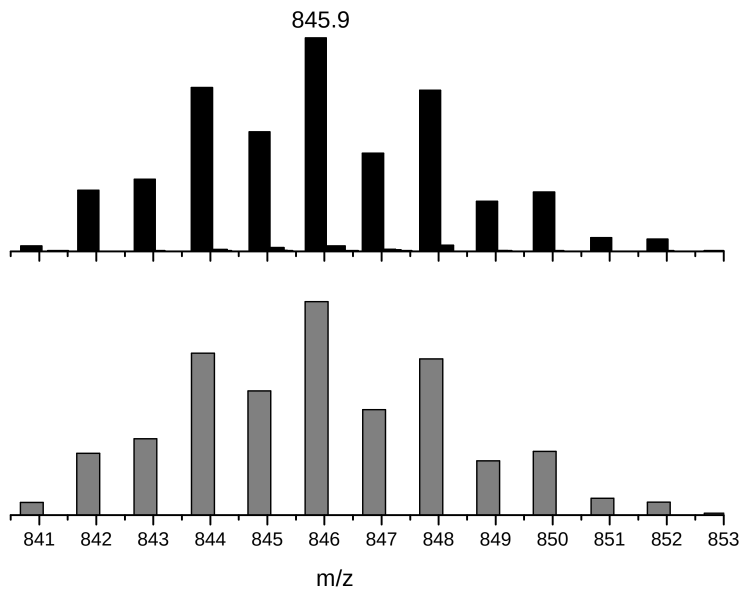
845.9
841
842
843
844
845
846
847
848
849
850
851
852
853
m/z

(c)

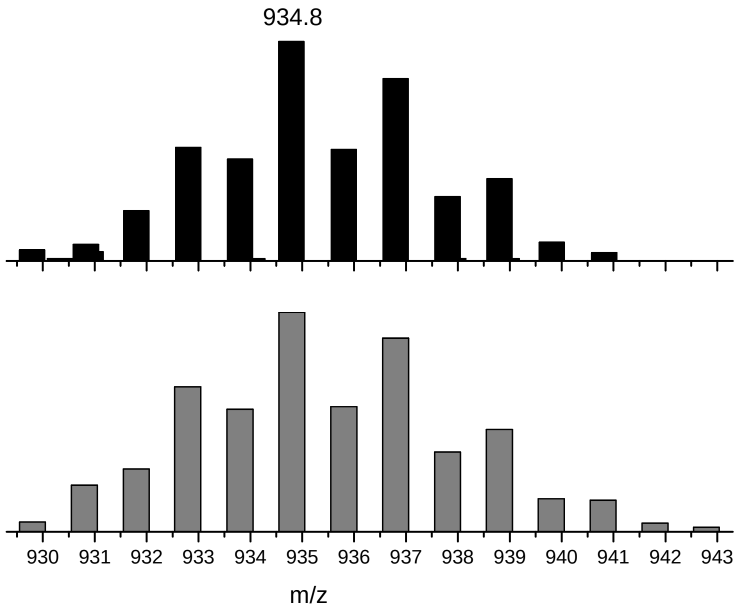
934.8
930
931
932
933
934
935
936
937
938
939
940
941
942
943
m/z

(d)

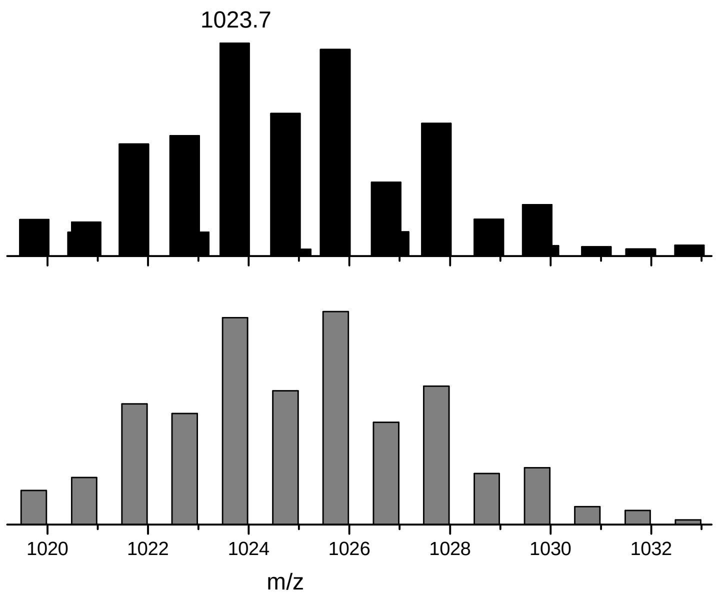

(e)

Fig. S8 (a) The negative-ion ESI mass spectrum of [Tp*WS_3Cu_3(μ_3-DMF)$(CN)_3$Cu]·2$(DMF)_{0.5}$. (b) The observed patterns (up) and the calculated isotope patterns (bottom) of the [Tp*$WS_3Cu_2(CN)_2]^-$ anion (at m/z = 756.9). (c) The observed patterns (up) and the calculated isotope patterns (bottom) of the [Tp*$WS_3Cu_3(CN)_3]^-$ anion (at m/z = 845.9). (d) The observed patterns (up) and the calculated isotope patterns (bottom) of the [(Tp*WS_3Cu_3)Cu$(CN)_4]^-$ anion (at m/z = 934.8). (e) The observed patterns (up) and the calculated isotope patterns (bottom) of the [(Tp*WS_3Cu_3)$Cu_2(CN)_5]^-$ anion (at m/z = 1023.7).

The third-order NLO measurements of 1−5

The solutions of **1** (6.0×10^{-5} M), **2** (6.0×10^{-5} M), **3** (6.0×10^{-5} M), **4** (6.0×10^{-5} M), and **5** (6.0×10^{-5} M) in DMF were placed in a 1.5 mm quartz cuvette for the third-order NLO measurements. These five compounds were stable toward air and laser light under experimental conditions. As a reference, the optical nonlinearity of the standard sample CS_2 was also observed. The third-order NLO properties were measured using femtosecond DFWM technique with a Ti:Sapphire laser (Spectra-physics Spitfire Amplifier). The pulse width was determined to be 80 fs on a SSA25 autocorrelator. The operating wavelength was centered at 800 nm. The repetition rate of the pulses was 1 kHz. During the measurement the laser was very stable (rms < 0.1%). The input beam was split into two beams k_1 and k_2 with nearly equal energy by use of a beam splitter (BS) and then focused on a plot of the sample. The beam k_2 passed through a delay line derived by a stepping motor in order that the optical path length difference between the k_2 and k_1 beams could be adjusted during the measurement. The angle between the beams k_1 and k_2 were about 5°. When k_1 and k_2 were overlapped spatially in the sample, the generated signal beam k_3 passed through an aperture, recorded by a photodiode and then analyzed by a lock-in amplifier and computer.

Details of the equations used in calculations of third-order NLO properties

The third-order nonlinear optical susceptibility $\chi^{(3)}$ is measured *via* a comparison with that of a reference sample CS_2, calculated from the DFWM signal (I), the linear refractive index (n), the sample thickness (L) and absorption correction factor using eq. 1:[1]

$$\chi_s^{(3)} = \left(\frac{I_s}{I_r}\right)^{1/2} \cdot \frac{L_r}{L_s} \cdot \left(\frac{n_s}{n_r}\right)^2 \cdot \frac{\alpha \cdot L \cdot \exp(\alpha L/2)}{1-\exp(-\alpha L)} \cdot \chi_r^{(3)} \qquad (1)$$

where the subscripts "*s*" and "*r*" represent the parameters for the sample and CS_2. And α is the linear absorption coefficient. The last fraction comes from the sample absorption and equals to 1 while the sample has no absorption around the employed laser wavelength. The values of $\chi_r^{(3)}$ and n_r for CS_2 are 6.7×10^{-14} esu and 1.632, respectively.[2]

The third-order nonlinear refractive index n_2 in isotropic media is estimated through eq. 2:[3]

$$n_2(esu) = \frac{12\pi\chi^{(3)}}{n^2} \qquad (2)$$

where n is the linear refractive index of the solution.

The second-order hyperpolarizability γ of a molecule in isotropic media is related to the solution $\chi^{(3)}$ by Equation (3):[4]

$$\gamma = \frac{\chi^{(3)}}{N f^4} \qquad (3)$$

where N is the number density of the solute per milliliter, and f^4 is the local field correction factor which is $[(n^2 + 2)/3]^4$ (n is the linear refractive index of solution).

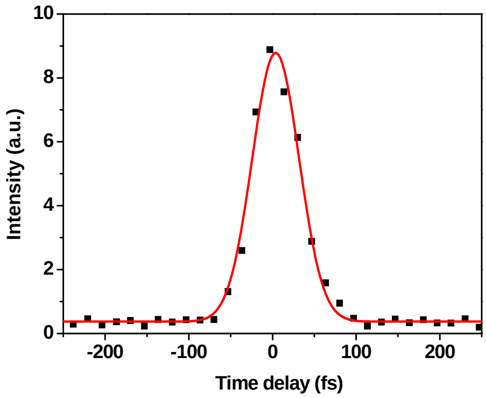

(a)

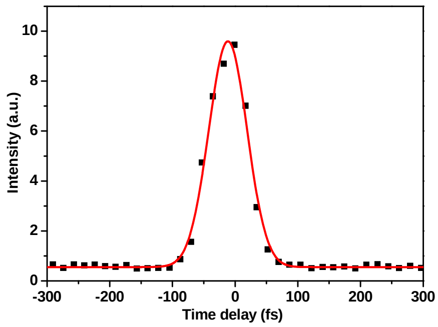

(b)

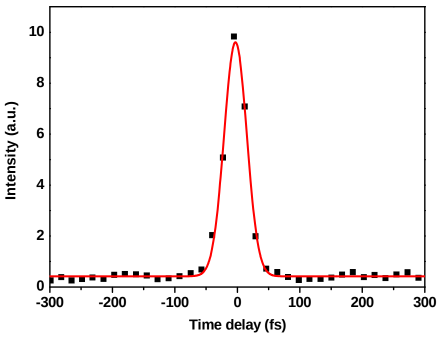

(c)

Fig. S9 The DFWM signal for the DMF solutions of 6×10^{-5} M for **2**(a), **3**(b) and **4**(c) with 80 fs and 1.5 mm cell. The black solid squares are experimental data, and the red solid curves theoretical fit.

Table S1 Selected bond lengths (Å) for **2–5**[a]

	Complex **2**		
W(1)-N(8)	2.268(10)	W(1)-N(6)#1	2.284(7)
W(1)-N(6)	2.284(7)	W(1)-S(1)	2.301(3)
W(1)-S(2)	2.304(3)	W(1)-S(2)#1	2.304(3)
W(1)-Cu(2)	2.6444(17)	W(1)-Cu(1)	2.6589(12)
W(1)-Cu(1)#1	2.6590(12)	Cu(1)-C(1)	1.870(10)
Cu(1)-S(1)	2.219(3)	Cu(1)-S(2)	2.222(3)
Cu(1)-O(1)	2.490(5)	Cu(2)-O(1)	2.679(10)
Cu(2)-C(2)	1.885(13)	Cu(2)-S(2)#1	2.209(3)
Cu(3)-N(2)#2	1.971(13)	Cu(3)-N(1)	1.992(11)
Cu(3)-N(1)#3	1.992(11)	Cu(3)-N(3)	2.093(16)
S(1)-Cu(1)#1	2.219(3)	N(2)-Cu(3)#2	1.971(13)
Cu(2)-S(2)	2.209(3)		
	Complex **3**		
W(1)-N(4)	2.293(7)	W(1)-N(4)#1	2.293(7)
W(1)-N(6)	2.296(9)	W(1)-S(2)	2.306(3)
W(1)-S(1)#1	2.308(2)	W(1)-S(1)	2.308(2)
W(1)-Cu(1)	2.6560(18)	W(1)-Cu(2)#1	2.6614(11)
W(1)-Cu(2)	2.6614(11)	Cu(1)-C(1)	1.814(14)
Cu(1)-S(1)#1	2.223(3)	Cu(1)-S(1)	2.223(3)
Cu(1)-O(1)	2.499(10)	Cu(2)-O(1)	2.563(3)
C(2)-Cu(3)	1.898(8)	N(1)-Cu(3)#2	1.961(15)
N(2)-Cu(2)	1.902(9)	S(1)-Cu(2)	2.227(2)
S(2)-Cu(2)	2.218(3)	S(2)-Cu(2)#1	2.218(3)
Cu(3)-C(2)#3	1.897(8)	Cu(3)-N(1)#4	1.961(15)
	Complex **4**		
W(1)-N(8)	2.273(9)	W(1)-N(6)	2.276(8)

W(1)-N(10)	2.297(9)	W(1)-S(3)	2.306(3)
W(1)-S(1)	2.306(3)	W(1)-S(2)	2.313(3)
W(1)-Cu(3)	2.6607(15)	W(1)-Cu(2)	2.6637(15)
W(1)-Cu(1)	2.6698(15)	Cu(1)-C(1)	1.904(11)
Cu(1)-S(1)	2.222(3)	Cu(1)-S(2)	2.232(3)
Cu(1)-O(1)	2.391(9)	Cu(1)-Cu(3)	2.961(2)
Cu(1)-Cu(2)	2.990(2)	Cu(2)-C(2)	1.892(11)
Cu(2)-S(3)	2.222(3)	Cu(2)-S(2)	2.226(3)
Cu(2)-Cu(3)	2.974(2)	Cu(3)-C(3)#1	1.914(10)
Cu(3)-S(1)	2.225(3)	Cu(3)-S(3)	2.227(3)
Cu(4)-N(3)	1.917(12)	Cu(4)-N(1)	1.925(12)
Cu(4)-N(2)#2	1.983(13)	N(2)-Cu(4)#2	1.983(13)
C(3)-Cu(3)#3	1.914(10)		

Complex **5**

W(1)-N(6)	2.274(9)	W(1)-N(10)	2.282(9)
W(1)-N(8)	2.285(9)	W(1)-S(1)	2.304(3)
W(1)-S(3)	2.305(3)	W(1)-S(2)	2.312(3)
W(1)-Cu(1)	2.6579(17)	W(1)-Cu(3)	2.6610(17)
W(1)-Cu(2)	2.6676(16)	Cu(1)-C(1)	1.883(12)
Cu(1)-S(2)	2.223(3)	Cu(1)-S(1)	2.228(3)
Cu(1)-Cu(3)	2.951(2)	Cu(1)-Cu(2)	2.964(2)
Cu(2)-C(2)	1.884(13)	Cu(2)-S(2)	2.215(3)
Cu(2)-S(3)	2.219(3)	Cu(2)-Cu(3)	3.002(2)
Cu(3)-C(3)	1.896(11)	Cu(3)-S(1)	2.210(3)
Cu(3)-S(3)	2.225(3)	Cu(4)-N(4)	1.904(11)
Cu(4)-N(1)#1	1.934(12)	Cu(4)-N(2)	1.974(12)
N(1)-Cu(4)#1	1.934(12)		

[a] Symmetry codes for **2**: #1 x, $-y + 1/2$, z; #2 $-x$, $-y$, $-z + 2$; #3 x, $-y - 1/2$, z; for **3**: #1 x, $-y + 3/2$, z; #2 $-x + 1/2$, $-y + 2$, $z - 1/2$; #3 x, $-y + 5/2$, z; #4 $-x + 1/2$, $-y + 2$, $z + 1/2$; for **4**: #1 $-x$, $y + 1/2$, $-z + 1/2$; #2 $-x$, $-y$, $-z$; #3 $-x$, y

– 1/2, –*z* + 1/2; for **5**: #1 –*x* + 1, –*y* + 1, –*z* + 1; #2 –*x* + 1, –*y*, –*z* + 2; #3 –*x* + 2, –*y* + 1, –*z* + 1.

References

(1) Yang, Y.; Samoc, M.; Prasad, P. N. *J. Chem. Phys.* **1991**, *94*, 5282−5290.

(2) Orezyk, M. E.; Samoc, M.; Swiatkiewicz, J.; Prasad, P. N. *J. Chem. Phys.* **1993**, *98*, 2524−2533.

(3) Jenekhe, S. A.; Lo, S. K.; Flom, S. R. *Appl. Phys. Lett.* **1989**, *54*, 2524−2526.

(4) Mandal, B. K.; Bihari, B.; Sinha, A. K.; Kamath, M.; Chen, L. *Appl. Phys. Lett.* **1995**, *66*, 932−934.